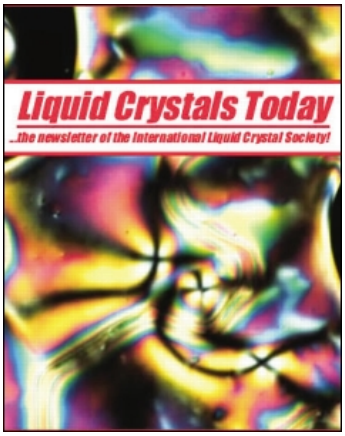

Liquid Crystals Today
Publication details, including instructions for authors and subscription information:
http://www.informaworld.com/smpp/title~content=t713681230

Colloidal inclusions in liquid crystals: Phase separation mechanisms and some dynamical aspects

J. C. Loudet[a]
[a] Centre de Recherche Paul Pascal, Avenue A. Schweitzer 33600 Pessac, France

To cite this Article Loudet, J. C.(2005) 'Colloidal inclusions in liquid crystals: Phase separation mechanisms and some dynamical aspects', Liquid Crystals Today, 14: 1, 1 — 14
To link to this Article: DOI: 10.1080/14625180500137803
URL: http://dx.doi.org/10.1080/14625180500137803

Liquid Crystals Today, Vol. 14, No. 1, March 2005, 1–14

Taylor & Francis
Taylor & Francis Group

Colloidal inclusions in liquid crystals: Phase separation mechanisms and some dynamical aspects

J.C. LOUDET

Centre de Recherche Paul Pascal, Avenue A. Schweitzer 33600 Pessac, France

(29 April 2005)

This article reviews recent findings on the formation of ordered colloidal structures from bulk demixing in liquid crystalline materials. In contrast to classical phase separations, which lead to randomly distributed macrodomains of various sizes, demixing in liquid crystals leads to remarkably uniform droplets that form ordered arrays of either infinitely long straight chains (nematic phase) or highly curved chains (cholesteric phase). This distinctive behaviour arises from the presence of topological defects and elastic distortions around the inclusions formed during the separation. These distortions induce long-range attractions and short-range repulsions. These forces direct the ordering of microdomains and stabilize them against coalescence, thereby limiting the coarsening mechanism of the separation. We show that the ordering can be controlled on a large scale by simply controlling the macroscopic alignment of the liquid crystal. We also discuss the influence of an electric field and demonstrate marked differences with classical emulsions and colloids in isotropic fluids. Finally, we analyse the Brownian fluctuations of an isolated droplet immersed in a nematic phase and derive a quantitative determination of the Stokes drag coefficients and their anisotropy.

1. Introduction

Phase separations from temperature quenches of binary mixtures start by the formation of small particles that grow and coarsen as time elapses [1]. In solid or liquid media, this coarsening leads to polydisperse dispersions of growing particles that eventually phase separate macroscopically. In the dilute limit of a liquid binary mixture, the domains of dispersed phase consist of droplets that exhibit Brownian motion and coalesce when they collide with each other. This classical scenario can be easily observed and is now rather well understood [1]. However, the situation can be completely different if the continuous phase exhibits liquid crystalline ordering. In that case, the droplets of the dispersed phase can still move upon Brownian motion, but the liquid crystal in which they are embedded induces long- and short-range forces that affect the separation and the structures formed at long times [2]. It has indeed been shown that colloidal inclusions in liquid crystals experience elastic forces mediated by the distortions of the liquid crystal ordering [3–21]. In the first part, we show that these forces, which do not exist in isotropic liquids, play a predominant role in phase separation mechanisms for they to anisotropic clusters and stabilize colloids. Instead of fully phase separating, the system self-stabilizes and self-organizes into highly ordered arrays of chains composed of monodisperse colloidal droplets [2]. The main features of this spontaneous ordering can be understood by considering elastic phenomena and topological defects around the droplets.

We then turn our attention to phase-separation experiments in a cholesteric liquid crystal continuous phase. These experiments provided us with another example of some of the unique structures that can be formed with liquid crystal-based colloidal systems. Addition of a small amount of chiral additives to a nematic liquid crystal can result in the formation of a cholesteric phase whose pitch is much larger than the observed droplet size during the phase separation. Even though the phase diagram and demixing process remain preserved because of the very small concentration of chiral additives, the final structures can be significantly different from those formed in a non-doped nematic. In a thin film of aligned cholesteric, the droplets self-organize into slightly twisted linear aggregates composed of a finite number of particles, instead of forming indefinitely long chains, as observed in classical nematics. In non-aligned films, larger aggregates, which consist of unique helical colloidal chains, can be observed. This behaviour, which can be understood by considering the cholesteric as a slightly twisted nematic, are in marked contrast with recent studies of other related systems. When the pitch is smaller than the particle size, the particles tend to stabilize networks of oily streak defects [22]. On the contrary, when the

Liquid Crystals Today
ISSN 1358-314X print/ISSN 1464-5181 online
http://www.tandf.co.uk/journals
DOI: 10.1080/14625180500137803

particles are very small (nanoparticles) they do not distort the long-range liquid crystal order and can surprisingly lead to the formation of new structures with a particular partition of the particles [23]. In the present study, the particles are of an intermediate size, i.e., they are large enough to distort the liquid crystal but sufficiently small to avoid the stabilization of defect networks.

As another distinctive feature in these systems, we summarize recent findings on the influence of an external electric field [24]. In classical isotropic emulsions and colloidal suspensions, an external field induces the polarization of the particles and their subsequent aggregation and coalescence because of dipole–dipole forces. Polarization of droplets and the resultant electrostatic dipole–dipole forces are also present in a liquid crystal. However, there are additional effects because of the modification of the liquid crystal alignment in response to the field. The latter not only induces a direct attraction, as in isotropic liquids, but also an indirect elastic repulsion by imposing different distortions and defects of the liquid crystal. This elastic repulsion can stabilize the droplets against coalescence – thereby leading us to the surprising conclusion that, in contrast to isotropic liquids, the phase separation can be arrested at will by applying an external field.

Finally, we report very recent results on some dynamical aspects of colloidal inclusions in a nematic liquid crystal [25]. Using video microscopy coupled with particle tracking routines, we experimentally determined the Stokes drag coefficients of a Brownian sphere immersed in the nematic phase. Besides being anisotropic, as predicted [26, 27], the viscous drag is further found to depend on the director configuration around the droplet. The results are in almost quantitative agreement with recent numerical computations [27].

The paper is divided into seven sections. In the next section, we recount some background details about the behaviour of colloidal inclusions in liquid crystals. We describe the distortions around inclusions and the resultant elastic interactions between them. Section 3 is devoted to experimental details related to the systems that allowed the mechanisms discussed in this paper to be observed. In section 4, we summarize the recently reported mechanisms of phase ordering from demixing in a nematic liquid crystal. We discuss the experimental observations using the concepts of the second section. The fifth section deals with more recent experiments of phase separation in a cholesteric continuous phase. We describe in section 6 the influence of an external electric field and demonstrate marked differences with the behaviour of classical electro-rheological fluids [28, 29]. Lastly, section 7 focuses on the Stokes drag determination of a Brownian sphere suspended in a nematic phase. A brief conclusion summarizes the main concepts and experimental results reviewed throughout this paper.

2. Theoretical concepts

2.1. *Distortions and defects around colloidal inclusions in a nematic liquid crystal*

The liquid crystals considered throughout this work are thermotropic nematic liquid crystals composed of rigid, rod-like organic molecules that possess long-range orientational order. The preferred direction of alignment of the molecules is specified by the unit vector field **n**, called the director [30, 31]. The presence of droplets in the nematic host induces long-range distortions of the director field and these distortions mediate strong elastic forces between the particles. This problem has been extensively studied both theoretically and experimentally [3–21]. Another important source of energy in these systems comes from the local interactions between the liquid crystal molecules and the interfaces of both the particles and the boundaries of the sample; this is the anchoring energy.

When the anchoring to a surface is strong, the director makes a well-defined angle with this surface, regardless of the resultant elastic distortions. In this limit, the boundary conditions of **n** are fixed. By contrast, in the limit of weak anchoring, the competition between anchoring energy and elastic distortions may result in different orientations of the director at the interface. The combination of the geometry and the boundary conditions impose global topological constraints that must be satisfied by the director field of the liquid crystal. This can lead to the formation of additional topological defects [30, 31] that play a crucial role in determining the elastic droplet–droplet interactions.

A particle with homeotropic anchoring of the nematic director is equivalent to a topological defect called a radial hedgehog, which creates radial distortions [31]. To satisfy the condition that the liquid crystal must be aligned at long range, a droplet could either nucleate a companion hyperbolic hedgehog (figure 1a), or a disclination ring of finite radius encircling the droplet in a 'Saturn-ring' configuration (figure 1b) [3–8, 11–13, 16–21]. The two droplet-defect assemblies satisfy the global boundary conditions imposed on the sample, since the director is homogeneously aligned far from the droplet.

When the preferential anchoring on a particle is planar, a tangential configuration is expected [11, 14, 15]. The global boundary conditions are met by the

creation of two surface defects, called boojums [32, 33], located at the poles of the particle. They are diametrically opposed, and aligned along the axis of the nematic phase. In this paper, we will not consider this particular geometry but will focus only on systems that exhibit preferential normal anchoring.

The energy scale of an elastic distortion around a particle is of order KR, where K is a typical elastic constant of the nematic liquid crystal [30, 31] and R is the radius of the particle. For a thermotropic liquid crystal, K is approximately 10^{-11} N [30], and for a colloidal particle, R is approximately one micron. Thus the energy scale is a few thousands k_BT, where k_B is the Boltzmann constant and T the temperature. As a result, the entropy of the particles is negligible compared to the elastic interactions. In these conditions, the structures formed due to attractive elastic interactions remain stable against thermal fluctuations. A quantitative account of the behaviour of the liquid crystal, and the topological defects that result upon addition of particles, can be obtained by considering the free energy of the system, F. In the absence of any external field and in conditions of strong anchoring, it consists only of a bulk and surface term

$$F = F_{el} + F_S = \int dV\, f_{el} + \int dS\, f_S. \tag{1}$$

F_{el} is the elastic Frank free energy which describes the slowly varying spatial distortions of the director. The free energy density f_{el} is a function of the elastic modes of deformation of a nematic liquid crystal and is given by [30, 31]

$$f_{el} = \frac{1}{2}\left[K_1(\operatorname{div} \boldsymbol{n})^2 + K_2(\boldsymbol{n}\cdot\operatorname{curl} \boldsymbol{n})^2 + K_3(\boldsymbol{n}\times\operatorname{curl} \boldsymbol{n})^2\right] \tag{2}$$

where K_1, K_2, and K_3 are the splay, twist and bend moduli, respectively. F_S is the surface free energy which takes into account the interactions of the director with boundaries. A classical expression for the surface free energy density f_S is [34]

$$f_S = \frac{W}{2}\left[1 - (\boldsymbol{n}\cdot\boldsymbol{s})^2\right]. \tag{3}$$

The unit vector **s** denotes some preferred orientation of the director at the surface, and W is the coupling constant which merely stands for the strength of the anchoring at the surface of the particle. It varies in the range 10^{-7}–10^{-3} J/m^2[35]. The director field adopted in each of the situations described above (see figure 1) follows from a minimization of the total free energy F under the constraint that **n** is a unit vector. Different approaches including an analogue to electrostatics and computer simulations have been used to study the nematic distortions around particles and the relative stability of hedgehogs versus Saturn rings [4–9, 12, 13, 16–19, 21]. It was shown that the particle-hyperbolic hedgehog pair behaves like a dipole at long range whereas the Saturn ring configuration has quadrupolar symmetry [4–21]. In the experiments reported on inverted nematic emulsions [9, 11], where surfactant-coated water droplets are dispersed in a nematic host, the dipole configuration is almost invariably observed for strong normal anchoring conditions and droplet radii of around 1 μm. In these conditions, the dipole seems to be more stable than the Saturn ring. The observed separation between the hyperbolic defect core and the droplet is a small fraction of the droplet radius, R. From optical microscopy observations, it was experimentally shown that $r_d/R = 1.2 \pm 0.1$, where r_d is the distance between the defect core and the centre of the particle. This is in good agreement with theoretical predictions [5, 7–9, 12, 13, 16, 19]. However, for sufficiently small particles or weaker anchoring strength W, the Saturn ring appears to be more stable than the dipole [8, 13, 19]. This allows weaker distortions in the volume of the sample whereas a penalty has to be paid at the surface of the particle because of a weak deviation from the normal. The so-called surface ring [8, 13] corresponds to a Saturn ring sitting directly at the surface of the particle. In the limit of very weak anchoring or very small particles, we can imagine that the nematic accommodates the particle without creating any additional defects and the director field distortions are smooth everywhere.

2.2. *Interactions between inclusions and structures*

The boundary conditions on each particle surface and at infinity control the nature and position of topological

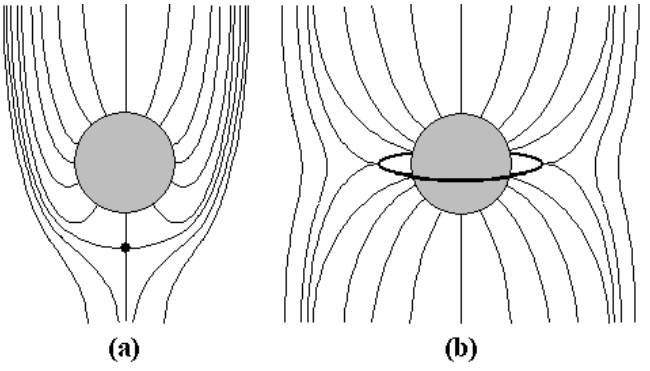

Figure 1. Schematic diagrams of the director field distortions (black lines) around particles in an aligned nematic liquid crystal (normal anchoring). (a) Dipole configuration. (b) Quadrupolar Saturn ring configuration.

defects around each particle. These in turn determine the far-field director distortions and the nature of the elastic droplet–droplet interactions [9, 11]. Because of its dipolar symmetry, the particle-hedgehog pair creates dipolar distortions of the director field at long range, leading to dipole–dipole interactions between drops that give rise to their chaining [2, 9–11]. The equilibrium distance of drops within a chain is set by the in-between hyperbolic hedgehog defect which prevents the droplets from contacting, thereby providing a short-range elastic repulsion [2, 9–11]. However, the amplitude and the anisotropy of the interactions between drops exhibiting the Saturn ring configuration are completely different. The quadrupolar symmetry leads to repulsive interactions when the line joining the centres of two particles makes an angle of 0° or 90° to the far-field alignment of the director [6, 7], taken as the z-axis. The particles repel each other when they are either perpendicular or aligned along the z-axis. It follows that the structures generated by quadrupolar interactions are significantly different from those generated by dipolar interactions. Instead of chain-like structures, more compact aggregates are formed [11, 14, 15]. In such aggregates, the droplets come into contact and there is no strong elastic repulsion. In inverted nematic emulsions, the stability of these structures is presumably ensured by the presence of surfactants at the water–liquid crystal interface [11].

Theoretically, the long-range two-body interactions of both dipolar and quadrupolar droplets can be determined through integration of a phenomenological free energy density containing f_{el}, plus symmetry-allowed terms which couple the director to particle concentration gradients [6, 9, 12, 20]. The electrostatic analogue [12], although elegant and efficient at providing qualitative guidelines, suffers from some limitations. It assumes a single elastic constant and is only valid at long range, i.e., at length scales where the particles can be viewed as point objects. At short range, more complex phenomena can govern the behaviour and structures of the particles.

3. Experimental details

In this section we present the materials and experimental procedures we have used to explore demixing phenomena in liquid crystals.

3.1. *Liquid crystals and silicone oils*

The system under study is a simple binary mixture composed of a silicone oil and a thermotropic liquid crystal forming the continuous phase. The silicone oils were provided by Aldrich (Aldrich, 37848-8, poly(dimethylsiloxane-co-methylphenylsiloxane)) and Fluka (Fluka, 85427-DC710, poly(dimethylsiloxane-co-diphenylsiloxane)). The liquid crystal is a eutectic mixture of cyanobiphenyl and cyanoterphenyl molecules and was provided by Merck (trade name 'E7'). Strictly speaking, since E7 is not a pure compound, our mixture may be viewed as a quasi-binary system. Pure E7 shows a typical first-order isotropic-to-nematic transition at about 62°C, as evidenced by microscopic observations in capillaries. The nematic phase of E7 is stable over a large temperature range around room temperature.

The cholesteric liquid crystal used in section 5 was obtained by adding a small amount (a few weight %) of cholesterol, an optically active substance, to the liquid crystal E7. Although not accurately measured, the cholesteric pitch is a fraction of a millimetre. We have not found any qualitative difference between samples with different pitches as long as the pitch remains much greater than the particle size.

3.2. *Sample preparation*

The mixture was heated to the isotropic phase (70°C) and stirred for a few minutes to ensure homogeneity. A thin cell, consisting of two glass slides separated by $20\,\mu$m thick spacers, was filled by capillarity in the isotropic phase with the binary mixture. But before the mixture was added, the glass slides were previously coated with polyvinylalcohol (PVA) and rubbed along a defined direction with a piece of velvet. This treatment causes the liquid crystal molecules to become homogeneously aligned parallel to the slides in the nematic phase (planar anchoring).

3.3. *Methods*

We have performed temperature quenches of the binary mixture from the pure nematic domain (N) to the diphasic domain (N+I) of the phase diagram (see figure 2) – quenches from the isotropic phase would have led to the formation of numerous and uncontrolled topological defects [36]. At 55°C, in the nematic phase, the liquid crystal was allowed to align for a few minutes. Once aligned, the system was quenched into the diphasic domain at 20°C by placing the sample onto a temperature-controlled stage of an optical microscope. At this temperature, phase separation occurs and as time evolves, the phenomenon can be easily pictured using a CCD camera attached to the microscope and connected to a frame grabber.

4. Phase separation in a nematic liquid crystal

In this section, we describe and explain the main aspects of a thermally induced phase separation of a binary

mixture containing a nematic liquid crystal forming the continuous phase. The scenario of the phase separation as well as the structures obtained at long times after the temperature quench are presented and discussed on the basis of the concepts recalled in section 2.

4.1. *Main features of a phase separation in a nematic liquid crystal*

We are interested here in systems where the liquid crystal forms the continuous phase of the binary mixture. The present discussion is based on the reported behaviour [2] of model systems composed of isotropic silicone oils in mixtures of cyano bi- and ter-phenyl liquid crystals in the limit of large fraction (>90 wt%) of liquid crystal. The system forms an isotropic (I) phase at high temperature, and a diphasic equilibrium between an isotropic and a nematic phase (I+N) at low temperature. A nematic reentrant domain (N) is found at intermediate temperatures and low silicone oil concentrations (see figure 2) [2, 37, 38].

When a sample is thermally quenched from the reentrant nematic domain to the diphasic domain, the uniform single-phase mixture is thermodynamically unstable and phase separation occurs. The first steps of the process are quite reminiscent of those taking place in mixtures composed of isotropic fluids [1]. Small isotropic particles, mostly composed of silicone oil, form and grow through coalescence as they diffuse and collide with each other. In classical mixtures, droplets varying noticeably in size are usually observed after a while. However, in the present case, a different phenomenon takes place when the coarsening silicone droplets reach a critical size, R^*, that is about a few microns. The coalescence is suddenly stopped and the droplets begin to attract one another, like electrostatic dipoles, to form small linear chains aligned along the nematic alignment direction [2]. We note that the use of a different silicone oil leads to different critical sizes (see below).

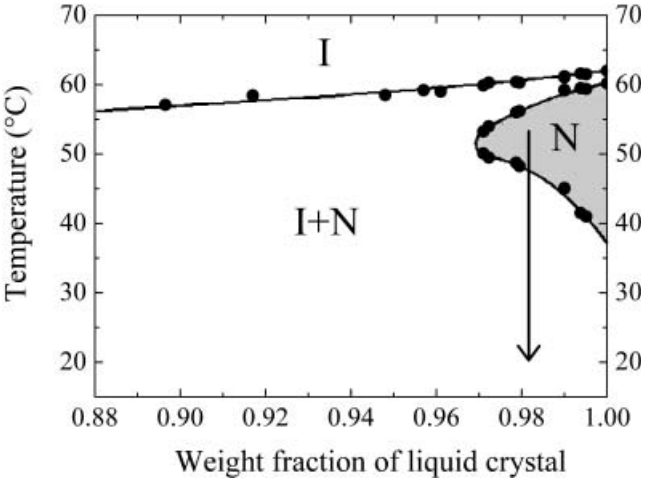

Figure 2. Partial phase diagram of the binary mixture liquid crystal E7/silicone oil (Aldrich). The systems are quenched from the nematic domain to 20 °C, as indicated by the arrow.

We also note that the silicone oils used have a density slightly lower than that of the liquid crystal. As a result, the oil particles tend to cream and lie closer to the upper slide than to the lower slide of the cell. The present phase separation can thus be considered as a two-dimensional process.

4.2. *Mechanism of separation*

In this subsection, our aim is to explain the main features of the phase separation described above. We first address the issues of stability, monodispersity of the particles and the formation of chains. In section 2, we saw that a spherical particle suspended in a liquid crystal tends to distort the long-range ordering of the director. Assuming a single elastic constant K for the nematic phase, the elastic cost of the distortions around a single particle should be of the order of KR, where R is the particle radius. These distortions, which mediate elastic interactions between the particles, depend critically on the boundary conditions at the surface of the particles. These boundary conditions are spontaneously set by molecular interactions between the liquid crystal molecules and the silicone oil interface. In our experiments, the preferential orientation of the liquid crystal molecules is normal to the oil interface. The characteristic energy specifying a deviation from this preferential alignment is given by WR^2, where W is a surface energy term which merely corresponds to the strength of the anchoring [4, 8, 12, 13]. The surface energy scales as R^2, whereas the bulk elastic energy scales as R. Thus, surface energy dominates over elastic energy for large drops whereas this is the opposite for small ones. This means that for drops typically larger than $R^* = K/W$, the liquid crystal molecules will preserve a normal orientation at the surface of the particle whatever the cost in terms of elastic energy. However, for drops typically smaller than R^*, we expect the surface director to deviate from its preferred alignment and adopt different orientations to minimize the bulk elastic distortions. From these considerations, we thus expect the distortions of the director to be size-dependent. This is exactly what happens in the experiments. At the early stages of the phase separation, the small droplets all exhibit the Saturn ring configuration as can be seen in figure 3. These floating quadrupoles can freely contact and coalesce since there is no elastic repulsion and no surfactant in the system. The

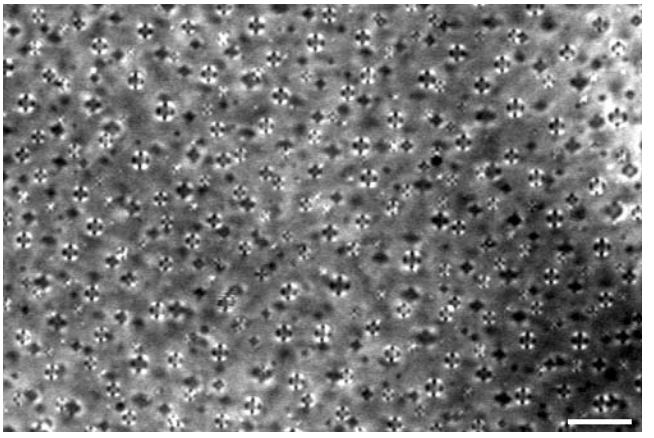

Figure 3. Early stage of the phase separation. The droplets exhibit four bright regions between crossed polarizers which is characteristic of quadrupolar distortions. All the droplets have the Saturn or surface ring configuration. System composition: liquid crystal, 96.5 wt%; siliconeoil (Fluka), 3.5 wt %. Scalebar: 9.9 μm.

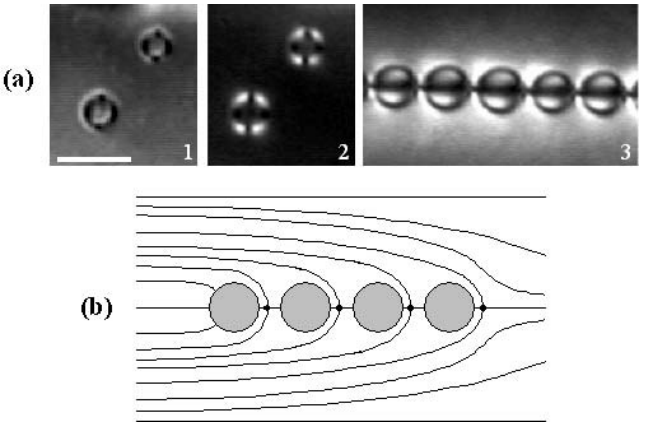

Figure 4. (a) Elastic dipoles and quadrupoles are easily recognizable between crossed polarizers since the director distorted regions differ in the two configurations. **1**: two quadrupoles between uncrossed polarizers. **2**: the same two quadrupoles between crossed polarizers. **3**: dipoles in a chain. Scale bar: 6.3 μm. (b) Schematic representation of a chain of dipoles.

coalescing quadrupoles therefore grow in size but the coalescence suddenly stops when they reach a well-defined characteristic size. We observe at this stage that the Saturn ring shrinks continuously to the hedgehog defect and transforms into the dipole configuration. The coalescence is inhibited as soon as the dipoles form because the companion hedgehog provides a short-range elastic repulsion as indicated above. The resulting elastic dipole–dipole interactions between drops lead to the formation of chains in which the droplet-defect pairs point in the same direction (figure 4). The chains follow the imposed nematic director alignment. This is why they are all oriented along a defined direction (figure 5). We stress that the transition between the Saturn ring and dipole configurations is sharp enough to lead to remarkably uniform dispersions. Assuming that W is of the order of $5 \cdot 10^{-6}$ J/m^2, a typical surface anchoring energy for cyanobiphenyl molecules and silicone materials [39], and that K is of the order of 10 pN [30], we expect the droplets to have a diameter $D(=2R^*)$ of about 4 μm, a value very close, as shown further, to that experimentally observed. This rough estimate provides additional support for the described mechanism.

From the above considerations, we expect the critical radius $R^*(=K/W)$ to change if either K or W varies. Since we keep using the same liquid crystal, changing the silicone oil is likely to affect the value of W. This is indeed what is observed experimentally with different silicone oils. Quadrupoles with diameters approaching 7.5 μm can be observed for the silicone oil provided by Fluka (see exp. section), which means that W is weaker in this case than with the silicone oil provided by Aldrich (see exp. section), for which D is about 3.5 μm. This is illustrated in figure 6. Dipoles begin to form when drops reach a critical diameter of about 7.5 μm for the Fluka oil. These observations prove that decreasing W tends to favour the Saturn ring over the dipole configuration, in agreement with previous experimental and theoretical work [8, 11–21].

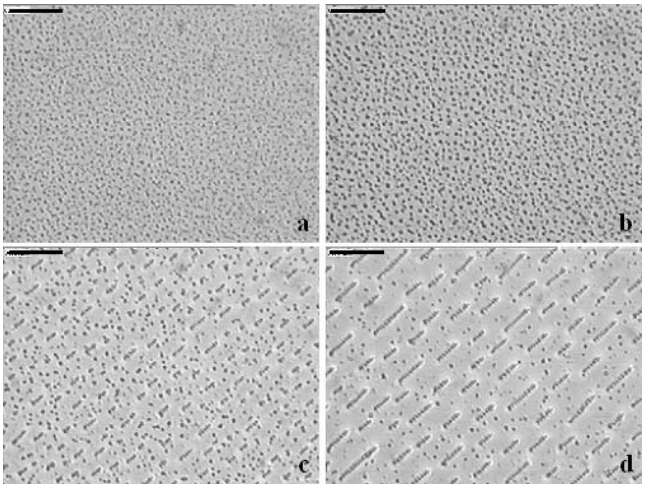

Figure 5. The phase separation process in a nematic solvent. System composition: liquid crystal, 98 wt%; silicone oil (Aldrich), 2 wt%. (a) Some droplets form after the quench (picture: 20 s after the quench). (b) The droplets diffuse randomly and coalesce in the initial stages of the phase separation (picture: 42 s after the quench). (c) Coalescence stops once a critical size is reached. The droplets begin to form small linear aggregates oriented along the alignment direction of the liquid crystal (picture: 55 s after the quench). (d) The chains grow as time evolves (picture: 120 s after the quench). Scale bar: 60 μm.

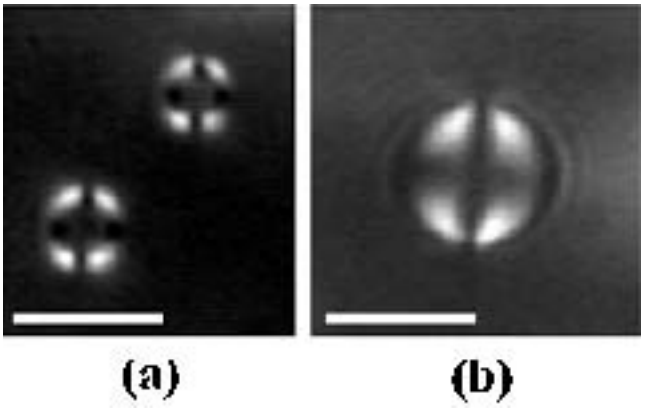

Figure 6. Bigger quadrupoles are observed with the Fluka oil (b) than with the Aldrich oil (a). These observations suggest that the anchoring strength, W, is weaker for the Fluka oil, leading to a bigger critical size, R^* (see text). We have measured $R^*_{\mathrm{Fluka}} \approx 4\,\mu$m while $R^*_{\mathrm{Aldrich}} \approx 2\,\mu$m. Scale bars: 5.8 μm.

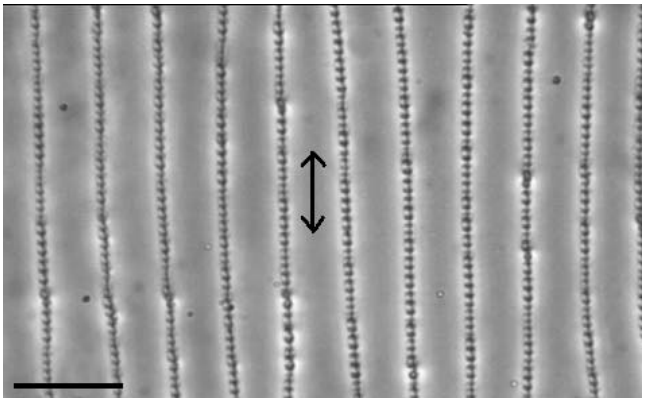

Figure 7. Very long chains are obtained at long times. They form highly ordered arrays made of monodisperse droplets. System composition: liquid crystal, 98 wt%; silicone oil (Aldrich), 2 wt%. Black arrow: direction of polymer rubbing. Scale bar: 50 μm.

For the two oils used, we found that the Saturn ring was more stable than the dipole configuration for drops typically smaller K/W. For drops larger than K/W, the dipole is the preferred configuration. These observations agree again with theoretical predictions [8, 12, 13].

We would like to point out here that the term 'Saturn ring' was constantly used to describe the quadrupolar distortions around drops. Although a surface ring has been predicted, it is rather difficult to discriminate between these two configurations because of the limited experimental resolution. It seems to us that the ring does not sit directly at the surface, at least for the biggest quadrupoles.

4.3. *Structures at long times*

As time elapses, the chains grow through 'tip to head' aggregation, and self-organize with respect to each other. At long times, typically 30 minutes after the quench, they form highly ordered arrays of macroscopic chains (several hundreds of microns long) made of monodisperse droplets which do not coalesce. An example of the resultant system is shown in figure 7. The samples remain in this state for months and even years. These observations are in marked contrast with the long-time behaviour of classical mixtures which usually fully phase separate [1]. The whole sample is filled with chains and the interchain distance d is uniform and decreases when the silicone oil concentration increases as shown in the plot of figure 8. This graph shows the variations of R^2/d, where R is the radius of the particles, as a function of ϕ, the weight fraction of silicone oil. Assuming that the weight fraction of the dispersed phase roughly corresponds to that of the silicone oil and considering that the chains span the whole surface area, R^2/d is expected to scale as ϕ. This is indeed what we observe. This behaviour proves the existence of a long-range repulsion between the chains. In the most concentrated systems, this repulsion leads to dislocation-like defects of the chain network in some parts of the sample (figure 9). These dislocations were the subject of a specific work [40] as an example of dislocations where rotational invariance is broken, in contrast to more classical dislocations encountered in smectics or cholesterics [30, 31]. Furthermore, the latter are generally thermally activated defects whereas in the present phase separation

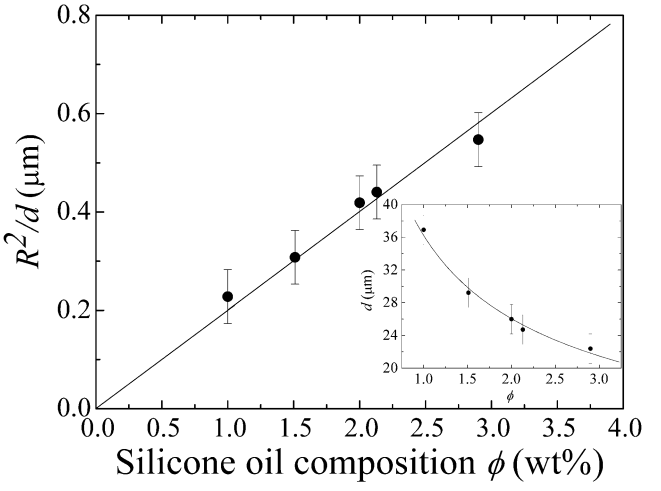

Figure 8. R^2/d against weight fraction of silicone oil, ϕ; R is the particle radius and d the separation between the chains. From mass conservation (see text), R^2/d is expected to scale as ϕ. The present data seem to confirm this behaviour which is an indication of a long-range repulsion between the chains. The solid line is a linear fit. Inset: values of d as a function of ϕ.

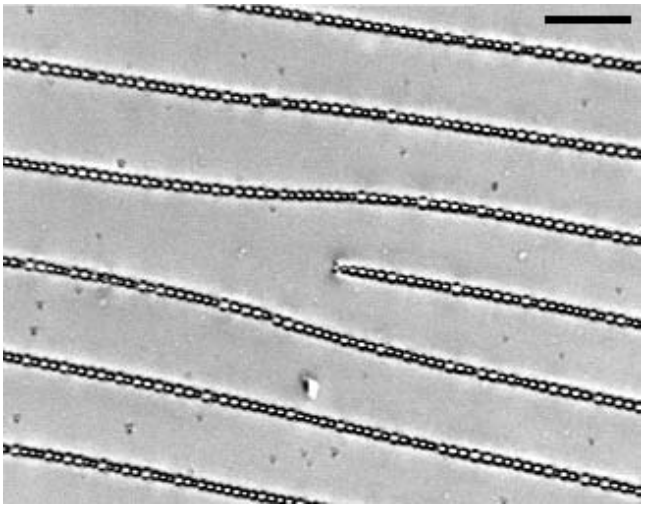

Figure 9. Isolated edge dislocation. System composition: liquid crystal, 98.4 wt%; silicone oil (Aldrich), 1.6 wt%. Scale bar: 30 μm.

experiments, the dislocations can be viewed as frozen defects whose origin can be understood *via* kinetic considerations [41].

5. Phase separation in a cholesteric liquid crystal

The experimental results presented so far deal with a nematic liquid crystal. In the previous section, we have seen that highly ordered arrays of chains are oriented along the nematic director alignment. Since the chains follow the director orientation, we could expect the chains to form twisted structures in a long-pitch cholesteric liquid crystal phase, i.e., a cholesteric phase with a pitch much larger than the colloidal inclusions. In the present conditions, the particles 'see' locally a nematic order. We stress that other behaviour can be observed when the pitch is on the order, or smaller, than the particles. Colloidal inclusions in a short-pitch cholesteric phase lead to the formation of an unusual particle-stabilized defect gel [22]. In the opposite limit, nanoparticles, much smaller than the cholesteric pitch, are partitioned in a peculiar way [23]. We have carried out temperature quenches of a binary mixture composed of a silicone oil (Aldrich) and a cholesteric liquid crystal. The latter was obtained by adding a small amount of cholesterol, an optically active substance, to the liquid crystal E7 [30]. Figure 10 shows the obtained structures in aligned and unaligned parts of the sample, respectively. The main difference deals with the orientation of chains. In aligned regions (figure 10a), we observe the formation of small chains, well-oriented along the z-axis. They are also very regularly spaced in the x-direction. We note that all the chains have curved ends which certainly arises from the weak director twist in these regions. These small chains do not attract one another to form longer chains as observed in nematics. They are composed of a few tens of droplets on average and this situation corresponds to a steady state. In unaligned regions (figure 10b), the chains follow the director structure and form long spirals that are either right-handed or left-handed. Even though these observations can be simply understood from what was already established in classical nematics; they provide a unique example of structures that could not be easily formed in other types of fields such as sedimentation, shear flow, electric or magnetic field.

6. Application of an external electric field

In this section, we discuss the behaviour of liquid crystal suspensions under the action of an external electric field. The behaviour of colloidal suspensions in electric

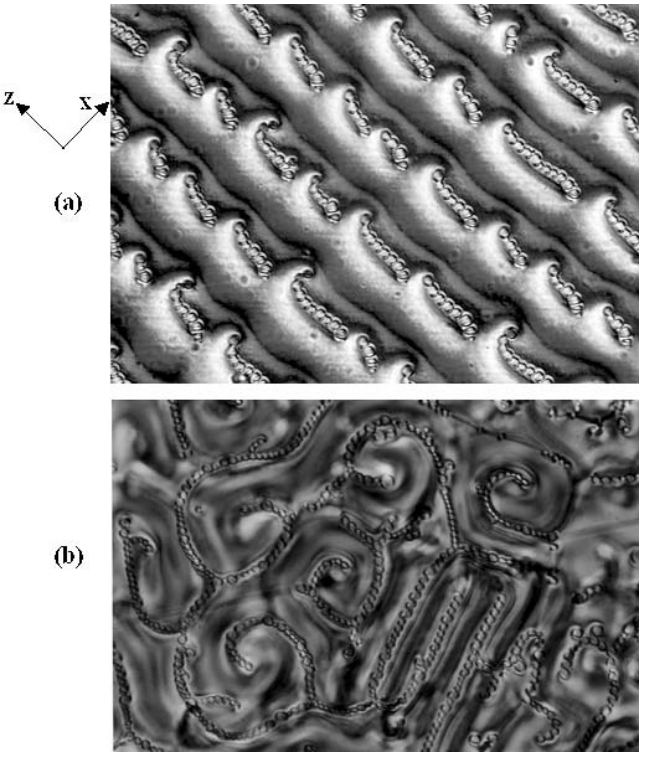

Figure 10. Phase separation in a cholesteric liquid crystal phase. (a) In aligned parts of the sample, small chains composed of monodisperse drops are observed. They are oriented along the z-axis and very regularly spaced along the x-axis. The weak director twist makes the chains have curved ends. In contrast with nematics, the small chains do not attract each other to form longer chains. They are composed of 5–10 drops only and correspond to the equilibrium state. (b) In unaligned parts of the sample, the chains form spirals due to the strong director twist. The helices can be either right- or left-handed. On both pictures, the droplets have a diameter that is about a few microns.

fields is of considerable technological interest with the so-called electro-rheological (ER) fluids [28, 29]. The main features of this behaviour are now rather well understood. When an external field is applied, particles suspended in an isotropic fluid become polarized. Resultant electrostatic dipole–dipole interactions between the particles lead to their chaining along the direction of the applied field. When suspended in a liquid crystal host, colloidal particles are also expected to be polarized upon the application of an electric field. However, new phenomena may take place because of the specific response of the liquid crystal. In this case, the external field is likely to alter the distortions of the liquid crystal alignment around the particles. These distortions induce elastic interactions between the particles and therefore play a crucial role in their stability and the formation of particular structures. In the absence of any external field, we know from sections 2 and 4 that elastic distortions in a nematic liquid crystal can have dipolar or quadrupolar symmetry depending on surface boundary conditions and droplet size. Different kinds of distortions and symmetries lead to completely different behaviours and structures. It is thus of critical importance to determine how the electric field affects the distortions around the particles. From a theoretical viewpoint, Stark predicted that an elastic dipole could be transformed into the quadrupolar Saturn ring configuration in the presence of an electric field [13]. Experimentally, Gu and Abbot [42], using cylindrically confined samples, have recently observed stable Saturn rings in the absence of a field and the expansion of the ring when the field is applied. Nevertheless, the transition predicted by Stark was not observed in these experiments. Here, we focus on more recent experimental results [24] which agree with Stark's theoretical predictions [13]. These experiments were performed in emulsions obtained from bulk demixing in liquid crystals as described in the previous sections. The systems used have a planar geometry, which may explain the differences from Gu and Abbot's experimental observations.

6.1. *Elastic dipole to elastic quadrupole transition*

The system we are interested in still consists of the binary mixture E7/silicone oil (Alrich or Fluka). As before, our experimental systems are all prepared by a thermally induced phase separation of this mixture. The experiments are performed in thin glass cells fitted with 50 μm thick spacers which served as electrodes. Their spacing is 1 mm and the field is applied in the plane of the cell. As the phase separation proceeds, it is possible to focus on an isolated particle before it interacts with its neighbours. We are primarily interested in the behaviour of the dipoles in the pressence of the field. If a high electric field (3–4 V/μm) is applied along the axis of an isolated elastic dipole, we observe a transition from the dipole to the quadrupole. Figure 11 shows the dipole point defect opening up into an equatorial ring which consists of a $-1/2$ disclination [31]. This opening is very quick and lasts less than a second (see figure 11b). It corresponds to a discontinuous transition between the dipole and the quadrupole and occurs only above a certain threshold field, E_S, which depends on the droplet size as well as on the anchoring strength [24]. These observations are quite in agreement with the simulations made by Stark [13]. Interestingly, a similar transition has been reported when an electric field is applied to nematic droplets suspended in isotropic phases. A hedgehog defect located at the centre of the drop loses its stability in the presence of the field and transforms into a ring at the surface of the drop [43].

While the field is on, the Saturn ring configuration is maintained and appears to be the most stable

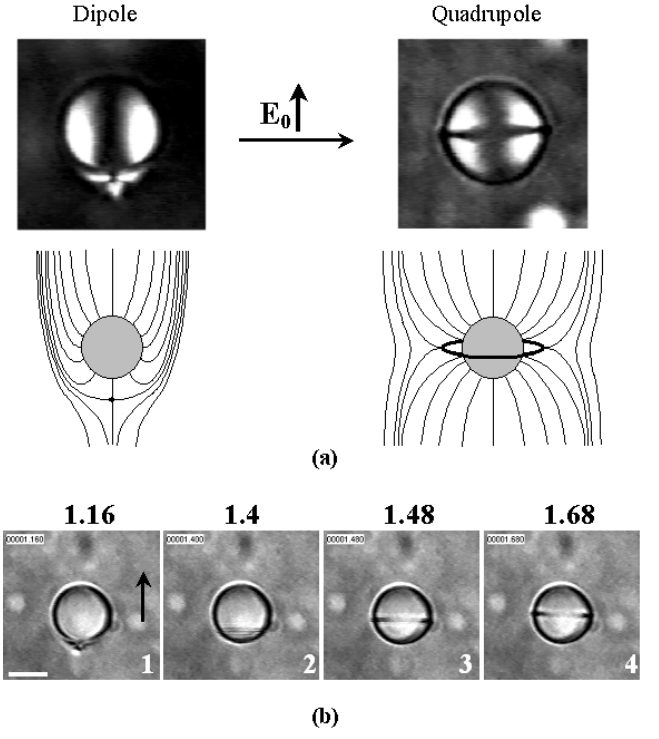

Figure 11. (a) Dipole to quadrupole transition in the presence of an electric field $\mathbf{E}_0$ applied along the dipole axis. The pictures were taken between crossed polarizers and the schematics below each picture show the associated director distortions. Drop diameter: 8 μm. (b) Sequence of images illustrating the opening of the hedgehog defect into a disclination ring: **1** dipole; **2** right after the opening; **3** off-centred ring; **4** Saturn ring. Black arrow: applied field direction. The black digits above each picture indicate the time in seconds. Scale bar: 7.6 μm.

configuration in the presence of the field. However, when the field is turned off, the ring continuously shrinks back to the hyperbolic hedgehog defect within a time scale of a few tens of seconds on average. This relaxation phenomenon, which is illustrated on figure 12, is hence much slower than the defect opening. The ring closing velocity is not constant but strongly increases whilst approaching the hedgehog defect (figure 13) [44]. In the absence of the field, the dipole configuration is always recovered and this observation proves that the dipole is stable against the quadrupole in our experimental conditions. Moreover, this behaviour shows that the predicted metastability barrier between the two configurations is weak or does not even exist in our experiments [12, 13]. From these experimental data, it is possible to numerically estimate the energy dissipation, E, during the ring relaxation. Within appropriate approximations, this energy is expected to be directly related to the previously calculated Frank elastic free energy when going from the quadrupole to the dipole. The calculation yields to a reduced dissipated energy $\bar{E}=E/\pi KR$ ranging from about 10 to 14 [44] while the reduced Frank energy variation, $\Delta\bar{F}=\Delta F/\pi KR$ (K is the nematic elastic constant and R the particle radius), is close to 2 [12, 13, 19].

6.2. *Elastic quadrupolar repulsion*

At the very beginning of the phase separation, we saw that the droplets exhibit the Saturn ring configuration. The system is strongly unstable since these floating quadrupoles attract one another due to attractive elastic quadrupolar interactions and freely coalesce. Application of a weak electric field E_0 ($E_0<1$ V/μm) at this moment polarizes the droplets and induces electrostatic dipole–dipole interactions between the quadrupoles which assemble into chains, exactly like in ER fluids. In those chains, the vector joining the centres of two drops, **r**, is parallel to the director alignment far from the drop. In such a configuration, the theory predicts that the quadrupoles experience an elastic repulsion [6, 8]. This is indeed verified experimentally.

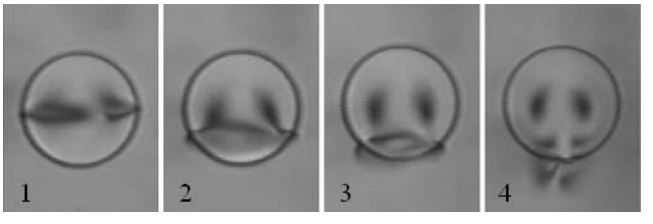

Figure 12. Series of pictures showing the ring defect relaxation once the electric field has been turned off. **1** Saturn ring; **2** and **3** intermediate configurations; **4** dipole. Drop diameter: 35 μm.

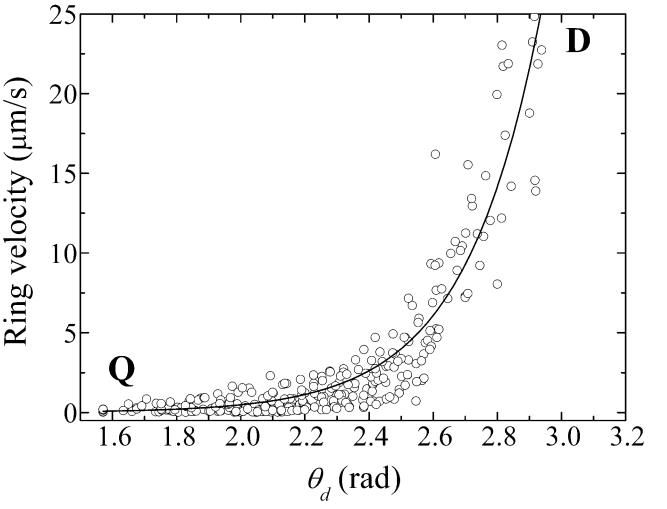

Figure 13. Ring closing velocity as a function of the opening angle θ_d, which describes the transition from the quadrupole (letter **Q**, $\theta_d=\pi/2$) to the dipole (letter **D**, $\theta_d=\pi$). The black solid line is just a guide to the eye.

There is a competition between the attractive electrostatic force, which forces the drops to come in close contact, and the repulsive elastic force which tends to drive them apart. This elastic repulsion is clearly evidenced in the sequence of images of figure 14. In picture **a**, the quadrupoles are close to one another but they do not touch each other. When the electric field intensity is decreased, these quadrupoles begin to move away from each other because of the elastic repulsion. For these field values (reported in figure 14), the elastic repulsion dominates the electrostatic attraction. For each field value E_0, an equilibrium distance between drops is set by the condition $\mathbf{F}_{elastic}=-\mathbf{F}_{elec}$. It is then possible to directly measure this elastic quadrupolar

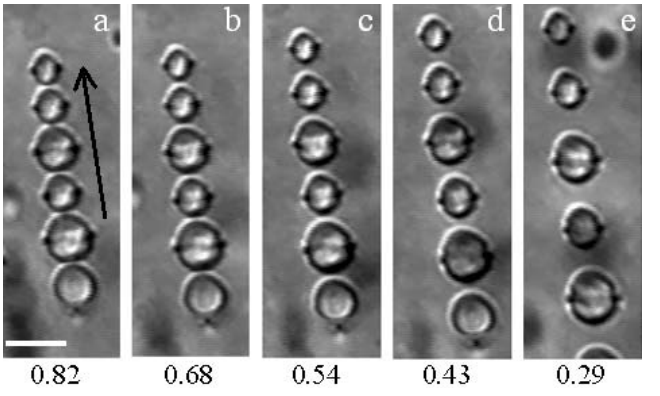

Figure 14. Evidence of the elastic quadrupolar repulsion. When the field intensity decreases, the droplets begin to be driven apart. The digits below each picture indicate the values of $\mathbf{E}_0$ in V/μm. Black arrow: direction of the applied electric field. Scale bar: 6.3 μm.

repulsion by measuring the centre-to-centre distance, r, between two drops of a chain for each E_0. A typical force profile is presented on figure 15. This graph illustrates how elastic quadrupoles actually repel each other when they are oriented in this configuration. On the y-axis of this graph, the quantity E_0^2/r^4 corresponds to the electrostatic force expression between two aligned electrostatic dipoles [45]

$$F_{\text{elec}} = 2F_0 \left(\frac{D}{r}\right)^4 \tag{4}$$

with $F_0 = 3\pi\epsilon_0\epsilon_s D^2\beta^2 E_0^2/16$ and

$$\beta = \left(\frac{\epsilon_p - \epsilon_s}{\epsilon_p + 2\epsilon_s}\right).$$

D is the diameter of the drops, ϵ_0 the dielectric permittivity of free space, ϵ_p the dielectric permittivity of the silicone oil particles and ϵ_s the dielectric permittivity of the liquid crystal solvent. As a first approximation, we set $\epsilon_s = \bar{\epsilon}_{LC}$, where $\bar{\epsilon}_{LC}$ is the mean dielectric constant of the liquid crystal [30]. Therefore, we deduce $F_{\text{elec}} \propto E_0^2/r^4$. Taking $\epsilon_p = 2.24$ [Aldrich source] and $\epsilon_{LC} = 8.7$ [46] at 1 kHz (frequency of the applied electric field), a crude estimate of the repulsive elastic interaction leads to force values around a few pN.

We stress that, in the absence of the field, the system is highly unstable since the quadrupoles freely coalesce. Then, our observations lead to the surprising conclusion that initially unstable particles can be stabilized by application of an electric field, provided that the particles are driven in a particular direction along which they repel each other. In a classical isotropic fluid, the electric field would tend to destabilize the system following the attraction and a subsequent coalescence of the drops.

In the absence of the field, previous theoretical predictions based on a long-range calculation predicted that the elastic quadrupolar repulsion force should follow the power law $F_{\text{elastic}} 1/r^6$ [6, 8]. Under the present experimental conditions, i.e., in the presence of an electric field, we observe a steeper repulsion as shown by the log–log plot in the inset of figure 15. Two reasons might explain the discrepancy between the experimental measurements and the theory. First, since the electric field is likely to distort the ordering of the liquid crystal molecules in the vicinity of the drops, the measured quadrupolar repulsion may intrinsically depend on E_0. Second, short-range effects, not considered in the theoretical approach, may come into play in the experiments. Indeed, the maximum measured separation between two drops is of order D.

Let us now consider again picture **a** of figure 14. If E_0 is increased to values ranging from 2 to 3 V/μm, we observe that the quadrupoles come into contact and further coalesce despite the elastic repulsion evidenced above. Indeed, for these field values, the attractive electrostatic force completely overwhelms the elastic repulsion force which eventually leads to a one-dimensional coalescence of the drops as shown in figure 16. Thus, the system is again unstable in the presence of high electric fields. Depending on the field intensity, we can then control the droplet coalescence and thereby their size.

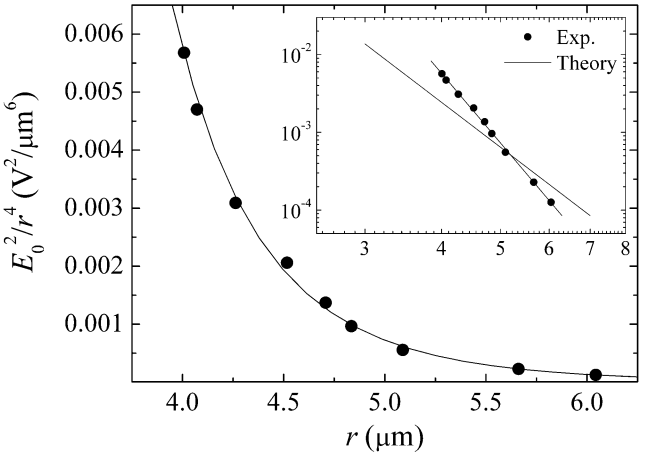

Figure 15. Quadrupolar elastic force $F_{\text{elastic}} \propto E_0^2/r^4$ as a function of the centre-to-centre distance, r, in the presence of an electric field. The force profile is repulsive and steeper than the long-range prediction in the absence of field (inset). A power-law fit leads to a scaling close to $1/r^9$ (solid line).

7. Brownian motion and Stokes drag

In this last section, we turn our interest towards some dynamical physical properties of colloidal inclusions in liquid crystals. We present very recent experimental

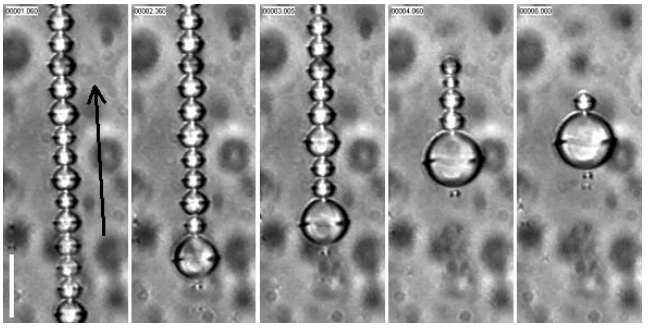

Figure 16. For $E_0 > 1$ V/μm, the electric field dominates the elastic repulsion and the quadrupoles are forced to coalesce within the chains. Black arrow: direction of the applied electric field. Scale bar: 14.1 μm.

results concerning the determination of Stokes drag coefficients of a Brownian sphere immersed in a nematic liquid crystal phase [25]. We then discuss the results in light of the currently available models.

The viscous drag of a sphere in an isotropic liquid was calculated by G. Stokes during the 19th century, in 1851. A sphere of radius R moving in a fluid of viscosity η experiences a Stokes drag force $F_S=6\pi\eta Rv$, where v is the velocity of the sphere [47]. The first theoretical studies of this problem in anisotropic liquids came out about 20 years ago [48–50] and it is still the subject of active theoretical and numerical investigations. For anisotropic liquids, an anisotropic drag force is predicted [27, 26]. Unlike previous falling-ball experiments [27], which can only yield to an average viscous drag, we use video microscopy coupled with particle tracking routines [51] to quantitatively measure the anisotropic diffusion coefficients.

The system under study is still the binary mixture composed of the liquid crystal E7 and a silicone oil (Aldrich). The samples are prepared by phase separation following the previously described procedure. Here, we focus on the early stages of the phase separation when the small coarsening oil droplets exhibit the Saturn or surface ring configuration where a disclination line surrounds the sphere at its equator (see figure 1b or schematics in figure 17). As aforementioned, this configuration is stable against thermal fluctuations and has quadrupolar symmetry.

Working with very dilute suspensions ($\phi_{oil}\leq 0.6$ wt%), these non-interacting quadrupoles, whose diameter ranges from 1 to 2 μm, perform Brownian motion. Using video microscopy and particle tracking routines [51], it is possible to analyse the Brownian fluctuations and get the particle positions at regular time steps. A typical trajectory derived from 1000 snapshots taken every 0.125 s is shown in figure 17. The self-diffusion coefficient of a random walker is given by the Stokes–Einstein relation $D=k_BT/6\pi\eta R$, where k_B is the Boltzmann constant and T the temperature [31]. Stokes drag forces can therefore be computed provided that D (and hence η) can be experimentally determined. Since the nematic phase has a rotational symmetry axis, the Brownian motion is governed by two independent diffusion coefficients, namely $D_{\|}$ and $D_{\perp}$, which characterize the diffusion along and perpendicular to the director respectively. They are given by $D_{\|/\perp}=k_BT/6\pi\eta_{\|/\perp}R$, where $\eta_{\|}$ and $\eta_{\perp}$ are related to the intrinsic viscosity coefficients of the liquid crystal material [27, 26].

From the analysis of the Brownian fluctuations, it is possible to derive $D_{\|}$ and $D_{\perp}$. The probability that a particle will diffuse a distance δ in the plane in time τ

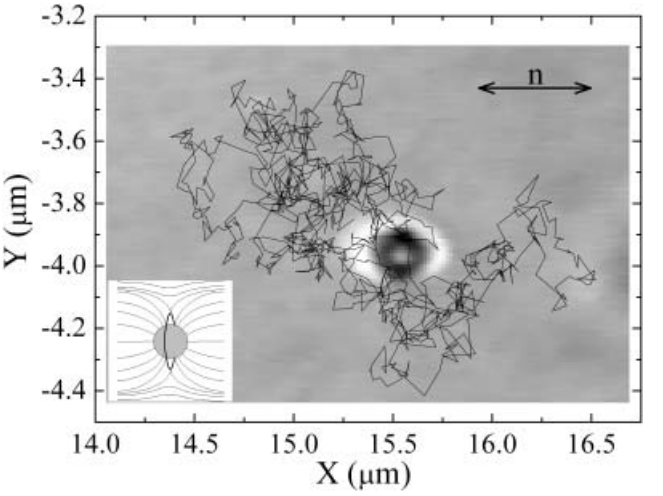

Figure 17. Brownian trajectory of a 1 μm diameter droplet embedded in a nematic continuous phase. Time τ between two steps: 0.125 s. Background picture: the director around the drop exhibits the Saturn ring configuration (see schematics) and the black double arrow indicates the director alignment far from the particle. The particle size and the graph axes do not have the same scale.

obeys the Gaussian distribution [31]

$$P(\delta|\tau)=P_0(\tau)\exp\left(-\frac{\delta^2}{\Delta^2(\tau)}\right) \qquad (5)$$

where $P_0(\tau)$ is a normalization constant and $\Delta(\tau)$ the width of the distribution. Averaging over 18 000 trajectory steps, figure 18 shows the histograms of the particle displacements $\delta=|\mathbf{r}(t+\tau)-\mathbf{r}(t)|$ in both the x ($\|\mathbf{n}$) and y ($\perp\mathbf{n}$) directions. The histograms are well fitted by a Gaussian distribution whose width, Δ, is directly related to D through $\Delta^2_{\|/\perp}=4D_{\|/\perp}\tau$. We see that $\Delta_{\|}>\Delta_{\perp}$ which implies that $D_{\|}>D_{\perp}$. It is therefore easier for the quadrupoles to diffuse along the director than perpendicular to it, as could be expected intuitively. From the values of $\Delta_{\|/\perp}$, we compute $D_{\|}$, $D_{\perp}$ and the anisotropy ratio $D_{\|}/D_{\perp}$ (see table 1). The results reported here for the Saturn ring configuration are in fair agreement with recent Stokes drag computations which take into account the distortions of the director field [27, 26]. These computations were performed in the limit of low Ericksen numbers, Er, defined as the ratio of viscous and elastic forces [30]. $Er\ll 1$ means therefore that the elastic deformation forces in the director field greatly exceed the viscous forces in the liquid so that the director field is not affected by the flow field. This latter condition was largely satisfied in the present experiments. For a uniform director field around the sphere, the calculations predict an anisotropy ratio of 2 [27], a value never observed in the experiments which

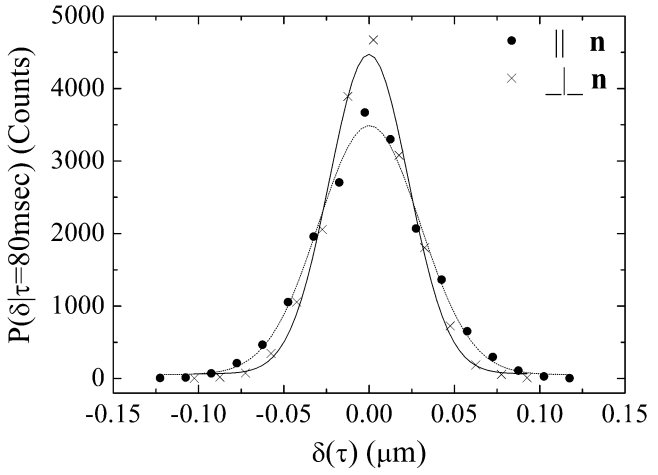

Figure 18. Histograms of particle displacements (see text) along (||) and perpendicular ($\perp$) to the director for $\tau=0.08$ s from a sample of 18000 trajectory steps. The solid and dotted lines are Gaussian fits.

Table 1. Diffusion coefficients and anisotropy ratios derived from experiments and simulations (see [27], values of 5CB) for a Saturn ring droplet of radius $R=0.55\,\mu$m.

	Experiments	Simulations
$D_{\|}[10^{-3}\,\mu m^2/s]$	7.7	7.9
$D_{\perp}[10^{-3}\,\mu m^2/s]$	4.8	4.6
$D_{\|}/D_{\perp}$	1.6	1.72

invariably lead to a value centred around 1.6 for particles of approximately the same size. The experiments then show that director field distortions and topological defects have to be taken into account for accurate Stokes drag calculations.

The Brownian fluctuations of the dipole configuration still remain to be investigated. However, since dipoles are bigger than quadrupoles in the present experimental conditions, preliminary experiments showed that it is much more difficult to probe accurately their Brownian fluctuations using the same video microscopy technique. According to the predictions though [27], the anisotropy ratio of the diffusion coefficients should not be so different to that found for quadrupoles.

In the opposite limit of high Ericksen numbers, a highly non-linear Stokes drag has been predicted for the dipole configuration [52] but has not received any experimental confirmation yet.

8. Conclusion

The results reported in this paper demonstrate that colloidal dispersions in thermotropic liquid crystals are novel challenging systems for discovering and studying new physical effects and structures. The anisotropy of the continuous phase leads to the observation of phenomena that are markedly different from those known in isotropic solvents. We have shown that a thermally induced phase separation of a binary mixtures containing a liquid crystal solvent and an isotropic oil does not lead to full phase separation. In a nematic liquid crystal, the mixture self-stabilizes and self-organizes into highly ordered arrays of infinite pearl chains. In a cholesteric liquid crystal, the director twist yields to the formation of twisted structures and spirals of chains, which cannot be easily achieved in other types of colloidal systems. In such systems, the size and spatial organization of the particles are controlled by the orientational elasticity and the topological defects of the continuous phase. We have also discussed the basics of the influence of an external electric field on these systems. The observed behaviour originates from the specific response of the liquid crystal to the applied field which alters the orientation of the molecules. Among the striking results, we first described an electric field-induced transition between an elastic dipole and an elastic quadrupole; followed by a relaxation phenomenon once the field is switched off. Surprisingly, we have seen that it is possible to stabilize an initially unstable dispersion by applying an electric field, behaviour in marked contrast to that of isotropic dispersions. Lastly, the analysis of the Brownian fluctuations of a sphere embedded in a nematic liquid crystal led us to the first experimental determination of the director field-dependent Stokes drag coefficients of a sphere.

Monodispersity, spatial ordering and absence of coalescence from phase separations in liquid crystals provide new and potentially helpful tools for the design of ordered composites and functional materials. The unusual behaviour of inclusions in the presence of an electric field could also be useful for the development of a new class of field-responsive fluids. To estimate practically the potential of these systems for future applications, it is now time to start exploring the physical properties of these materials. Little is known about their optical or rheological properties. They will presumably differ from those of classical emulsions. Several authors have recently started developing powerful algorithms able to simulate the behaviour of two or more particles in two dimensions [53–55] as well as the director dynamics around isolated particles [56]. The extension of these promising simulations to more complicated actual situations should pair up with new experiments to test them. We hope that the overall results will contribute to extending the great richness of colloidal liquid crystal systems and motivate further studies to explore their expected original properties.

References

[1] J.M. Gunton, M. San Miguel, P.S. Sahni. in *Phase Transition and Critical Phenomena,* vol. **8** (ed. J. L. Lebowitz) 267, Academic Press, London (1983).
[2] J.C. Loudet, P. Barois, P. Poulin. *Nature*, **407**, 611 (2000).
[3] P. Poulin, V.A. Raghunathan, P. Richetti, D. Roux. *J. Phys. II France*, **4**, 1557 (1994).
[4] E.M. Terentjev. *Phys. Rev. E*, **51**, 1330 (1995).
[5] O.V. Kuksenok, R.W. Ruhwandl, S.V. Shiyanovskii, E.M. Terentjev. *Phys. Rev. E*, **54**, 5198 (1996).
[6] S. Ramaswamy, R. Nityananda, V.A. Raghunathan, J. Prost. *Mol. Cryst. Liq. Cryst.*, **288**, 175 (1996).
[7] R.W. Ruhwandl, E.M. Terentjev. *Phys. Rev. E*, **55**, 2958 (1997).
[8] R.W. Ruhwandl, E.M. Terentjev. *Phys. Rev. E*, **56**, 5561 (1997).
[9] P. Poulin, H. Stark, T.C. Lubensky, D.A. Weitz. *Science*, **275**, 1770 (1997).
[10] P. Poulin, V. Cabuil, D.A. Weitz. *Phys. Rev. Lett.*, **79**, 4862 (1997).
[11] P. Poulin, D.A. Weitz. *Phys. Rev. E*, **57**, 626 (1998).
[12] T.C. Lubensky, D. Pettey, N. Currier, H. Stark. *Phys. Rev. E*, **57**, 610 (1998).
[13] H. Stark. *Eur. Phys. J. B*, **10**, 311 (1999).
[14] O. Mondain-Monval, J.C. Dedieu, T. Gulik-Krzywicki, P. Poulin. *Eur. Phys. J. B*, **12**, 167 (1999).
[15] P. Poulin, N. Francès, O. Mondain-Monval. *Phys. Rev. E*, **59**, 4384 (1999).
[16] D. Andrienko, G. Germano, M.P. Allen. *Phys. Rev. E*, **63**, 041701 (2001).
[17] J. Fukuda, H. Yokoyama. *Eur. Phys. J. E*, **4**, 389 (2001).
[18] R. Yamamoto. *Phys. Rev. Lett.*, **87** (7), 075502 (2001).
[19] H. Stark. *Phys. Rep.*, **351**, 387 (2001).
[20] B.I. Lev, S.B. Chernyshuk, P.M. Tomchuk, H. Yokoyama. *Phys. Rev. E*, **65**, 041709 (2002).
[21] J. Fukuda, M. Yoneya, H. Yokoyama. *Phys. Rev. E*, **65**, 041709 (2002).
[22] M. Zapotocky, L. Ramos, P. Poulin, T.C. Lubensky, D.A. Weitz. *Science*, **283**, 209 (1999).
[23] M. Mitov, C. Portet, C. Bourgerette, E. Snoeck, M. Verelst. *Nature Materials*, **1**, 229 (2002).
[24] J.C. Loudet, P. Poulin. *Phys. Rev. Lett.*, **87**, 165503 (2001).
[25] J.C. Loudet, P. Hanusse, P. Poulin. *Science*, **306**, 1525 (2004).
[26] R.W. Ruhwandl, E.M. Terentjev. *Phys. Rev. E*, **54**, 5204 (1996).
[27] H. Stark, D. Ventzki. *Phys. Rev. E*, **64**, 031711 (2001).
[28] W.A. Bullough. . in Proc. 5th International Conference on ER fluids, MR Suspensions and Associated Technology, World Scientific, Singapore. (1996).
[29] M. Parthasarathy, D.J. Klingenberg. *Mater. Sci. Eng. R*, **17**, 57 (1996).
[30] P.G. De Gennes, J. Prost. in *The Physics of Liquid Crystals*. Oxford University Press, London (1994).
[31] P.M. Chaikin, T.C. Lubensky. in *Principles of Condensed Matter Physics*. Cambridge University Press, (1998).
[32] M. Kurik, O.D. Lavrentovich. *JETP Lett.*, **35**, 444 (1982).
[33] G.E. Volovik, O.D. Lavrentovich. *Sov. Phys. JETP*, **58**, 1159 (1983).
[34] A. Rapini, M. Papoular. *J. Phys. (Paris) colloq.*, **30**, C4–54 (1969).
[35] L.M. Blinov, A.Y. Kabayenkov, A.A. Sonin. *Liq. Cryst.*, **5**, 645 (1989).
[36] B. Yurke, A.N. Pargellis, I. Chuang, N. Turok. *Physica B*, **178**, 56 (1992).
[37] C. Shen, T. Kyu. *J. Chem. Phys.*, **102**, 556 (1995).
[38] F. Benmouna, L. Bedjaoui, U. Maschke, X. Coqueret, M. Benmouna. *Macromol. Theory Simul.*, **7**, 599 (1998).
[39] O.D. Lavrentovich, V.G. Nazarenko, V.V. Sergan, G. Durand. *Phys. Rev. A*, **45**, R6969 (1992).
[40] J.C. Loudet, P. Poulin, P. Barois. *Europhys. Lett.*, **54** (2), 175 (2001).
[41] J.C. Loudet, P. Barois, P. Auroy, P. Keller, H. Richard, P. Poulin. *Langmuir*, **20**, 11336 (2004).
[42] Y. Gu, N.L. Abbott. *Phys. Rev. Lett.*, **85**, 4719 (2000).
[43] V.G. Bodnar, O.D. Lavrentovich, V.M. Pergamenshchick. *Sov. Phys. JETP*, **74**, 60 (1992).
[44] J.C. Loudet, O. Mondain-Monval, P. Poulin. *Eur. Phys. J. E*, **7**, 205 (2002).
[45] D.J. Klingenberg, C.F. Zukoski, J.C. Hill. *J. Appl. Phys.*, **73**, 4644 (1993).
[46] D. Lippens, J.P. Parneix, A.J. Chapoton. *J. Phys. (Paris)*, **38**, 1465 (1977).
[47] J. Happel, H. Brenner. in *Low Reynolds Number Hydrodynamics*. Klüwer Academic Publishers, Dordrecht (1991).
[48] A.C. Diogo. . Mol. Cryst. *Liq. Cryst.*, **100**, 153 (1983).
[49] V.G. Roman, E.M. Terentjev. *Colloid J. USSR*, **51**, 435 (1989).
[50] H. Heuer, H. Kneppe, F. Schneider. *Mol. Cryst. Liq. Cryst.*, **214**, 43 (1992).
[51] J.C. Crocker, D.G. Grier. *J. Coll. Interf. Sci.*, **179**, 298 (1996).
[52] H. Stark, D. Ventzki. *Europhys. Lett.*, **57**, 60 (2002).
[53] R. Yamamoto. *J. Phys.: Condens. Matter*, **16**, S1945 (2004).
[54] J. Fukuda, M. Yoneya, H. Yokoyama. *Eur. Phys. J. E*, **13**, 87 (2004).
[55] J. Fukuda, H. Stark, M. Yoneya, H. Yokoyama. *Phys. Rev. E*, **69**, 041706 (2004).
[56] J. Fukuda, H. Stark, M. Yoneya, H. Yokoyama. *J. Phys.: Condens. Matter*, **16**, S1957 (2004).